energies

MDPI

Article

Minimum Power Input Control for Class-E Amplifier Using Depletion-Mode Gallium Nitride High Electron Mobility Transistor

You-Chen Weng [1], Chih-Chiang Wu [2], Edward Li Chang [1] and Wei-Hua Chieng [3,*]

[1] Department of Material Science and Engineering, National Chiao Tung University, Hsinchu 30010, Taiwan; mars751101@gmail.com (Y.-C.W.); edc@mail.nctu.edu.tw (E.L.C.)
[2] Mechanical and Mechatronics Systems Research Laboratories, Industrial Technology Research Institute, Hsinchu 31040, Taiwan; John.Wu@itri.org.tw
[3] Department of Mechanical Engineering, National Chiao Tung University, Hsinchu 30010, Taiwan
* Correspondence: whc@cc.nctu.edu.tw; Tel.: +886-3-571-2121 (ext. 55152)

Abstract: In this study, we implemented a depletion (D)-mode gallium nitride high electron mobility transistor (GaN HEMT, which has the advantage of having no body diode) in a class-E amplifier. Instead of applying a zero voltage switching control, which requires high frequency sampling at a high voltage (>600 V), we developed an innovative control method called the minimum power input control. The output of this minimum power input control can be presented in simple empirical equations allowing the optimal power transfer efficiency for 6.78 MHz resonant wireless power transfer (WPT). In order to reduce the switching loss, a gate drive design for the D-mode GaN HEMT, which is highly influential for the reliability of the resonant WPT, was also produced and described here for circuit designers.

Keywords: wireless power transfer; class-E amplifier; minimum power input control; D-mode; GaN HEMT; gate drive

Citation: Weng, Y.-C.; Wu, C.-C.; Chang, E.L.; Chieng, W.-H. Minimum Power Input Control for Class-E Amplifier Using Depletion-Mode Gallium Nitride High Electron Mobility Transistor. *Energies* **2021**, *14*, 2302. https://doi.org/10.3390/en14082302

Academic Editors: Ben Minnaert and Chunhua Liu

Received: 19 March 2021
Accepted: 15 April 2021
Published: 19 April 2021

1. Introduction

Class-E power amplifiers perform well in wireless power transfer (WPT) applications [1] because of their simple topology as well as high efficiency under zero voltage switching (ZVS) and zero voltage derivative switching (ZVDS) conditions. Thus, they have been used in various applications, such as battery charging [2], drones [3], LED lighting [4], and biomedicine [5]. Many studies have demonstrated the excellent performance of class-E power amplifiers [6,7], particularly when gallium nitride high electron mobility transistors (GaN HEMTs) are used [7–11]. GaN HEMTs provide high efficiency and performance due to their exceptional characteristics, such as low gate charge loss [7] and gate-source capacitance, which almost produce an ideal ZVS [8,9].

However, the performance of class-E power amplifiers is affected by load variation in addition to various non-ideal factors [12]. In response, different strategies have been proposed to optimize class-E amplifiers to increase operating efficiency and extend the transfer distance. These strategies involve a tuning couple [13]; the tuning duty ratio and frequency in relation to inductors and capacitors [14]; the control and compensation of variations in coupling and load impedance [10,11]; the coupling structure [15]; and the addition of transmitters [16,17]. In addition, a study proposed an analytical method that accounts for non-ideal factors (such as the inductance resistance, on resistance, and leakage current) in order to reduce the difference between calculated and actual values [18]. Moreover, although the use of GaN HEMTs in class-E power amplifiers improves efficiency and performance, a compatible and suitable gate driver must be designed to drive the GaN HEMT [19,20]. To this end, the charge pump gate drive presented by Ishibashi [20] is useful for driving the depletion (D)-mode GaN HEMT in a class-E amplifier.

Previous studies have proposed several laboratory-fabricated D-mode GaN HEMTs in cascade configurations [21,22]. To fully exploit the advantages of fabricated GaN HEMTs in class-E amplifiers, this study used a D-mode GaN HEMT with a charge pump gate driver. Specifically, in this study, the equivalent circuit of a class-E amplifier with a D-mode GaN HEMT was experimentally tested. In addition, based on the equivalent circuit, the characteristics of a fabricated D-mode GaN HEMT and the parameter of a compatible charge pump gate driver for the D-mode GaN HEMT were included in analyses to improve practicability. We continue on our work presented in [23] to optimize the operation for each scenario by using the proposed minimum power input control. The demo of the ZVS manual operation was provided in the previous article [23]. Previous studies have also proposed their own unique methods to achieve the high efficiency class-E power amplifier for WPT systems. The PTE of the TX-coil with an NIC [24] was much higher than that of a conventional WPT system. A class-E PA [25], based on the load-pull and impedance-transformation technique, showed a high-efficiency WPT for a wide load range. In this study, a simple look-up table, selecting the best combination and procedure of different duty cycles, frequencies, and VDDs, was used to yield a quick response and optimize efficiency in class-E amplifiers. This paper is organized as follows. The design of the D-mode GaN HEMT gate drive for the wireless power transfer is sensitive to parameters such as parasitic capacitances, output characteristic, transfer characteristic, and leakage current. Therefore, the fabrication conditions and parameters of the D-mode GaN HEMT are introduced in Section 2.1 in order to explain the design for a gate drive compatible with wireless power transfer. The design of the gate drive for the D-mode GaN HEMT is highly influential for the reliability of the resonant WPT. Taking into account the electrical characteristics of the fabricated D-mode GaN HEMT, the design of the charge pump gate drive for the D-mode GaN HEMT is presented in Section 2.2. Finally, the class-E amplifier with a charge pump gate drive circuit, and the proposed minimum power input control, are described in Sections 2.3 and 2.4. Section 3 presents the experimental verification of resonant WPT with minimum power input control, and the conclusions are presented in Section 4.

2. Materials and Methods

In our previous paper [23], the mathematical derivation of the ZVS control of a class-E WPT unit was proposed. As stated in [23], one of the critical issues for WPT is dealing with the switching loss of the GaN HEMT transistor. The switching loss is mainly caused by GaN HEMT characteristics, including the output parasitic capacitance Coss and the input parasitic capacitance Ciss. Hence, the D-mode GaN HEMT characteristics, which are provided in Section 2.1, must be carefully studied and examined before and after the packaging. Nevertheless, the parasitic capacitance variations between turn-on and turn-off are the dominant factor for the switching loss. Hence, the gate driver design methodology is provided in Section 2.2. The design of the charge pump gate drive for the D-mode GaN HEMT is critical for class-E WPT efficiency. With regard to the maximum power transfer, we need to understand how the impedance matching mechanism is adjusted through the resonant frequency ω_o, which is discussed in Section 2.4. Finally, we introduce a method called minimum power input control that functions by controlling the duty ratio δ, given in Section 2.5, to ensure the best power transfer efficiency (PTE), which implies the high PDL associated with a low switching loss. Figure 1 shows a flowchart of the key characteristic parameters for achieving the minimum power input control which is introduced in the following sections.

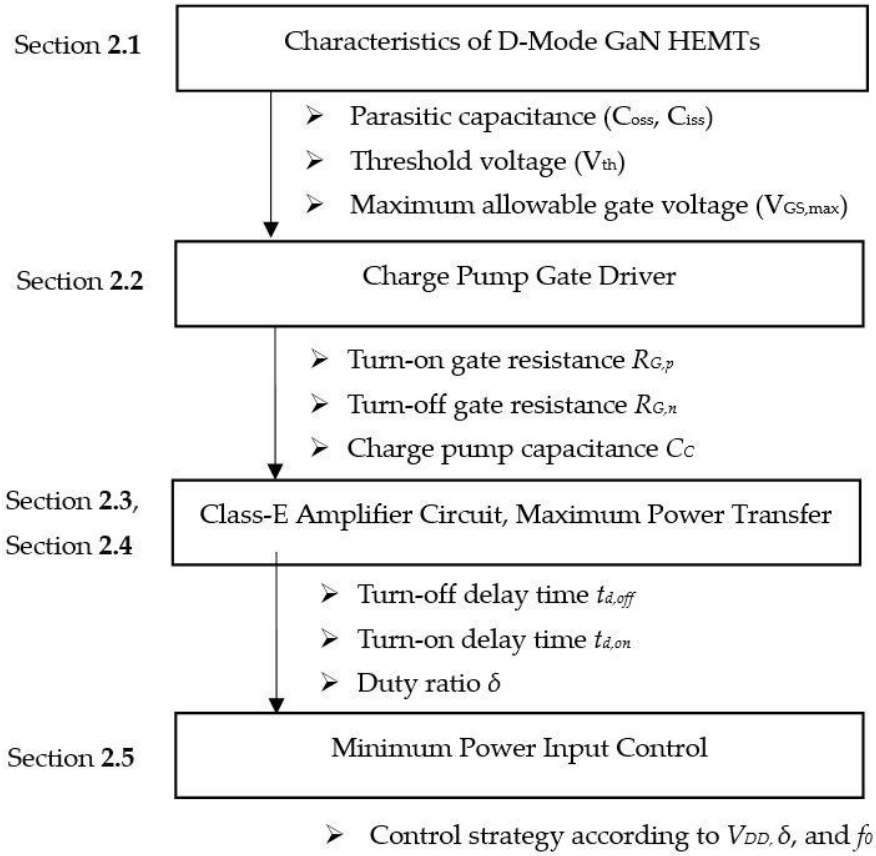

Figure 1. Flowchart of key characteristic parameters, which may also refer to [23], for achieving the minimum power input control.

2.1. D-Mode GaN HEMT

Figure 2a illustrates the transfer characteristics of the fabricated D-mode GaN HEMT device when $V_G = -10$ to 1 V, with $V_D = 10$ V in Figure 2b. The threshold voltage given by the tangent of the I_D–V_G was found to intersect at −7 V. Therefore, the turn-on voltage of the D-mode GaN HEMT, $v_{GS,ON}$, was recorded at −7 V. The maximum allowable gate voltage $V_{GS,max}$ was tested under the condition of $|V_{GS,max}| < 30$ V. According to the leakage current due to different voltages, $C_{OSS} = C_{GD} + C_{DS}$ varied, albeit only slightly, in the turn-on and turn-off periods. Furthermore, as the D-mode GaN HEMT had no body diode, the leakage current only flowed when v_{DS} was negative. Table 1 summarizes the characteristics of the D-mode GaN HEMT.

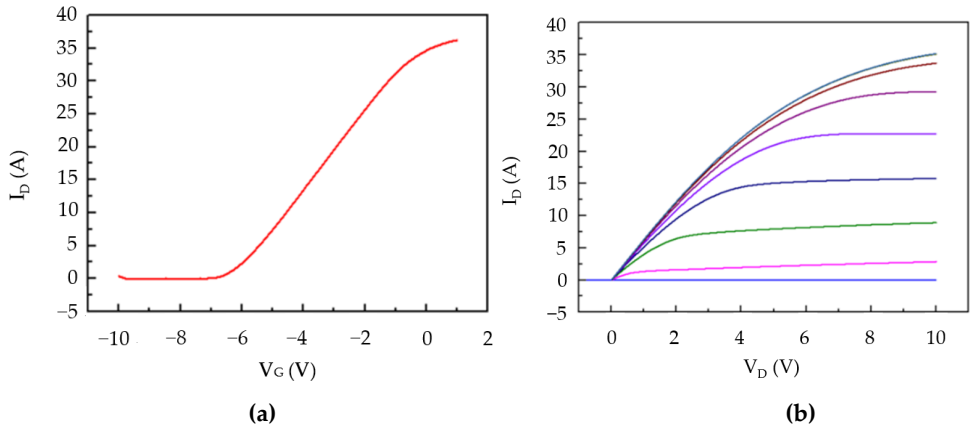

Figure 2. Characteristics of the D-mode GaN HEMT: (**a**) transfer characteristic; (**b**) output characteristic.

Table 1. Summary of characteristics of the D-mode GaN HEMT.

Symbol	Parameter	Value	Unit
$v_{GS,ON}$	Turn-on voltage	−7	V
C_{DS}	Drain-source parasitic capacitance	100	pF
C_{GD}	Gate drain Parasitic capacitance	80	pF
C_{GS}	Gate source Parasitic capacitance	420	pF
$V_{GS,max}$	Maximum gate-source voltage	8	V
$V_{DS,BD}$	Drain-source breakdown voltage	1000	V
$i_{d,max}$	Maximum drain current	35	A

The main reasons that the GaN HEMT is well-suited for WPT applications are that (1) it can perform high frequency switching with low switching loss; (2) it possesses no body diode; and (3) it involves low Ciss and Coss variation. The characteristic of have no body diode can ease the ZVS control and provide low energy loss during class-E switching operations. The Ciss and Coss variations of MOSFET can be as high as several hundred times between turn-on and turn-off. As for the GaN HEMT, Table 2 summarizes the parasitic capacitance of the D-mode GaN HEMT before packaging. The parasitic capacitances were nearly one-third of the MOSFET. The parasitic capacitance value and its variation were different for different packaging. For instance, the TO247, as shown in Figure 3b, yielded smaller capacitance than the TO220 shown in Figure 3a. Both types of packaging showed that the capacitance variation between turn-off at low V_{DS} and turn-on at high V_{DS} becomes smaller as the switching frequency increases. This is very good for resonant WPT in which the switching frequency is targeted at 6.78 MHz. In this study, the GaN HEMT in the TO220 packaging was used as it resulted in a smaller size than the TO247 packaging.

Table 2. The parasitic capacitances of the D-mode GaN HEMT.

Symbol	Parameter	Typical (pf)	Conditions
Ciss	Input capacitance	99.7	V_{DS} = 150 V, V_G = −10 V, T = 25 °C, 1 MHz
Coss	Output capacitance	9.2	
Crss	Transfer capacitance	7.1	

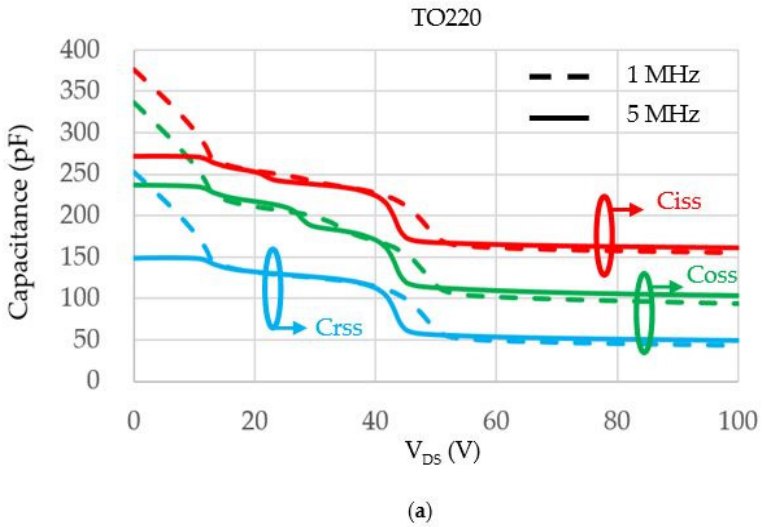

(a)

Figure 3. *Cont.*

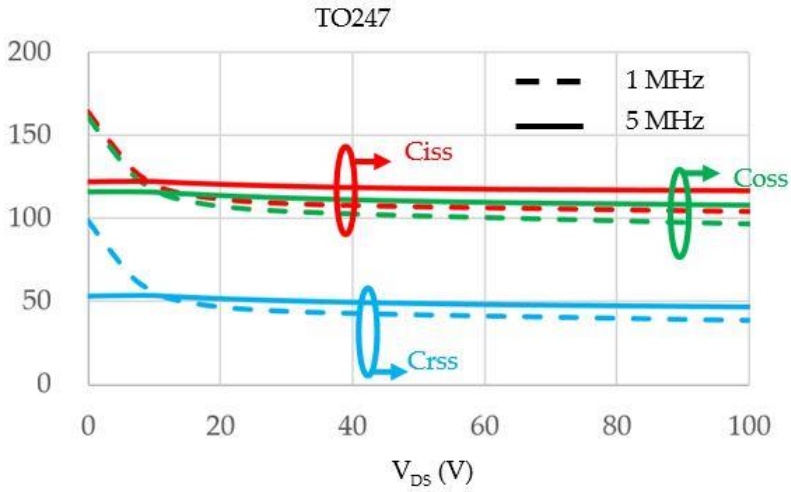

(**b**)

Figure 3. The parasitic capacitance of D-mode GaN HEMT via (**a**) TO220 and (**b**) TO247 packaging.

The design of the D-mode GaN HEMT gate drive for the wireless power transfer is sensitive to parameters including the gate-drain parasitic capacitance C_{rss} (=C_{GD}) and the gate input parasitic capacitance C_{iss} (=C_{GD} +C_{GS}). It is preferable for these parasitic capacitances to be as small as possible to enable higher frequency switching without much switching loss. On the other hand, the drain-source parasitic capacitance C_{DS} incorporated with C_2 and L_2 forms a useful LC tank for the power transfer unit (PTU), which needs to be as constant as possible during the time the transistor is switching on and off. All the parasitic capacitances are closely related to the GaN HEMT design, including the thickness of the epitaxial structure of the GaN device. The resulting output characteristic in Figure 2b determines the $R_{D,on}$ related to the efficiency of the wireless power transfer. The transfer characteristic in Figure 2a shows the preferable v_{GS} control range. It is preferable for the turn-on voltage $v_{GS,ON}$ to be as near to zero as possible to reduce the voltage level of the power supply for the gate drive.

2.2. Design of Charge Pump Gate Drive for D-Mode GaN HEMT

In order to design the D-mode GaN HEMT gate drive for class-E amplifiers, Ishibashi's [20] charge pump gate drive was adopted in this study. The leakage current is critical to the charge pump reservoir dynamics, which result from the reverse saturation current of the Schottky barrier diodes (SBD), which is preferably kept as small as possible. The disadvantage of the charge pump circuit—the current leaking through the diode reverse saturation current—causes no harm to the high frequency switching. However, the class-E amplifier has the additional disadvantage of C_{GD} being connected to the high voltage switching of v_{DS}.

In a p–n junction diode, two types of capacitance occur: transition capacitance (C_T) and diffusion capacitance (C_D):

$$C_{j0} = C_T + C_D, \quad (1)$$

In a forward-biased diode, C_D, which is the focus of the following derivation, is much larger than the C_T. Furthermore, the gate drive v_s is high, and the current i_G passes from V_{GH} to V_{SS}, which, for simplicity, is taken as the ground. The current i_G passes from V_{GL} to V_{SS} when v_s is low. As shown in Figure 4, we first assumed that V_{DS} is floating and that $R_{G,p} = R_G$. In the gate drive state, v_s is high and $v_{G,h}$ = 0.7 V, according to the diode forward-threshold voltage (built-in potential). The charge on the gate and diode side is:

$$Q_{G,h} = (C_{GS} + C_{j0}) \cdot v_{G,h}, \quad (2)$$

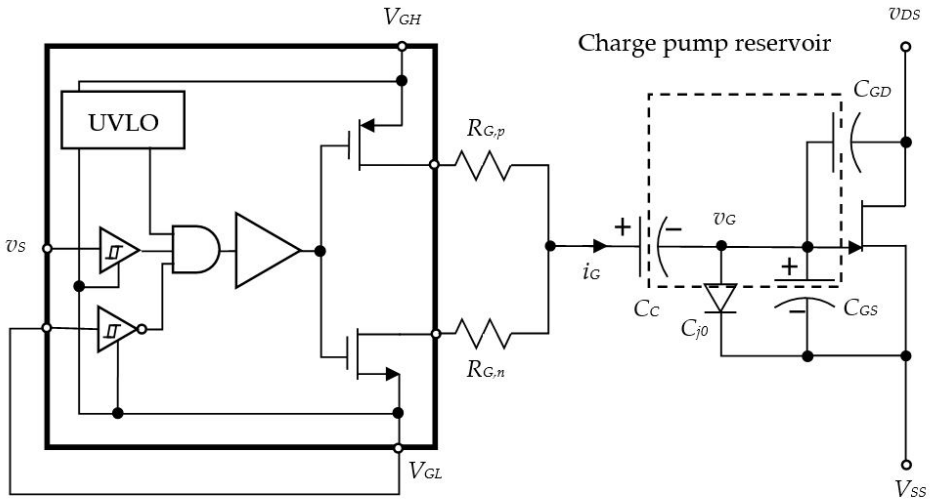

Figure 4. Charge pump gate drive design.

The charge on the capacitor side is:

$$Q_{C,h} = C_C \cdot (V_{GH} - v_{G,h}), \tag{3}$$

The steady state gate voltage when the gate is turning off is:

$$v_{G,l} = Q_{C,l}/(C_{GS} + C_{j0}) = -Q_{C,l}/C_C + V_{GL}, \tag{4}$$

Assuming that $C_C >> C_{GS} + C_{j0}$ and $V_{GL} = 0$ V, $v_{G,h}$ is small compared with V_{GH}.

$$Q_{C,l} \approx -C_C \cdot V_{GH}, \tag{5}$$

$$v_{C,l} \approx V_{GH}, \tag{6}$$

The leaking current in the charge pump occurs due to the diode reverse saturation current. When v_{DS} is connected to a half sine voltage such that

$$v_{DS} \approx 0 \text{ V when } v_s \text{ is high, } v_{DS} \approx V_{DS,max} sin(\omega_o t) \text{ when } v_s \text{ is low} \tag{7}$$

the charge pump requires some amount of negative charge, which must be quickly supplied, because of C_{GD} (the Miller capacitor) when v_{DS} is increasing to a high voltage and the gate is turning off. The charge pump must also retract the same quantity of negative charges when the gate is turning on. Thus, in such dynamic behavior, the resulting effect is the Miller plateau: a low voltage surge occurs when the gate is turning on, and the period in the Miller plateau increases when the gate is turning off. As shown in Figure 5, when $R_{G,p}$ is too high (as indicated by the dotted line), $R_{G,p}$ causes a negative voltage surge due to the rapid retraction of negative charges through C_{GD} and C_C to $R_{G,p}$. The negative voltage can potentially surge down to lower than $-V_{GS,max}$ and cause the gate source to break down. In such cases, $R_{G,p}$ must be reduced to prevent a large voltage drop in $v_{G,h}$ when the gate is turning on; the corresponding design parameters for the gate drive are shown in Table 3. The ideal gate source voltage for 6.78 MHz switching is also indicated by a dark solid line in Figure 5. Using the D-mode GaN HEMT as the switching device, the resonance mechanism for proper resonant frequency is a function of the duty cycle settings based on the hypotheses of zero voltage control and zero current control for the class-E amplifier [23]. ZVS and ZCS are achieved by adjusting both the duty cycle and resonant frequency to comply with the known phenomenon in GaN HEMT control, including the Miller plateau and current clamp in the gate drive design.

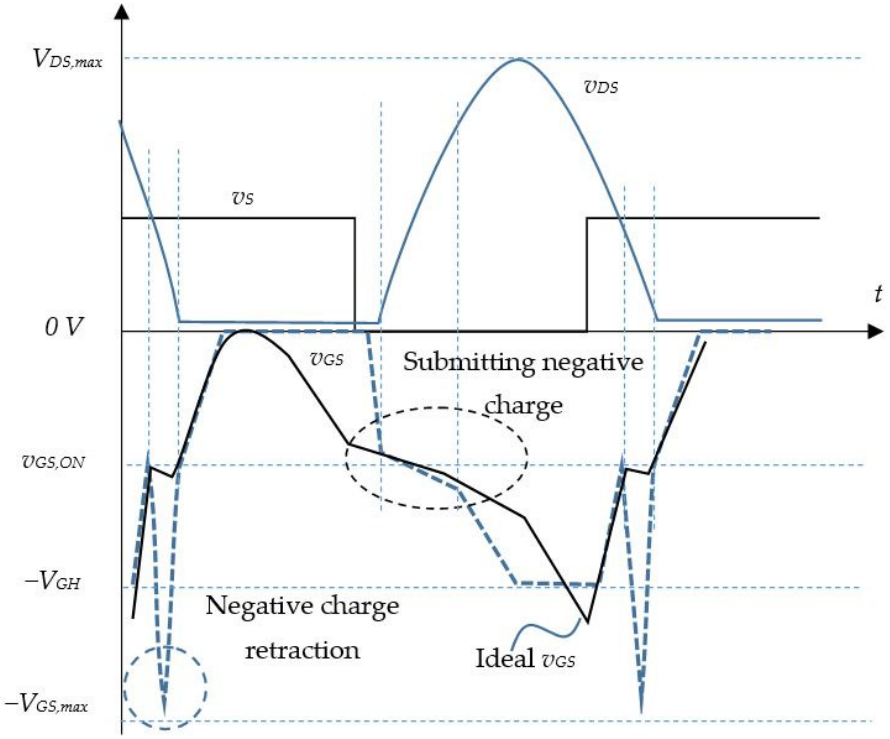

Figure 5. Gate response with high voltage v_{DS} effect from class-E amplifier.

Table 3. Parameters used in the charge pump gate drive.

Symbol	Parameter	Value	Unit
$R_{G,p}$	Turn-on gate resistance	12	Ω
$R_{G,n}$	Turn-off gate resistance	30	Ω
C_C	Charge pump capacitance	5	nF
C_{GS}	Diode capacitance	40	pF
I_R	Diode reverse saturation current	50	μA

2.3. Class-E Amplifier Circuit

Class-E amplifiers, as shown in Figure 6, have been used in 6.78 MHz resonant WPT applications. In this study, the actual load Z_L for a wireless power transfer system was considered to be the mutual inductance in parallel with the equivalent impedance of the receiver side. For simplicity in exposition, we let the load R_L be purely resistive. In the circuitry, the capacitor C_{DS} is the parasitic capacitor of the D-mode GaN HEMT. As the GaN HEMT contains no body diode, (1) a current path where v_{DS} is negative is impossible and (2) the resonant current i_2 can be sinusoidal with low total harmonic distortion (THD). In the equivalent circuit, the input and output power of the class-E amplifier are defined as $P_{in} = i_1 V_{DD}$ and $P_{out} = i_2 v_L$, respectively. The WPT experimental layout is shown in Figure 7a, and the charge pump gate driver for the D-mode GaN HEMT is shown in Figure 7b. The circuit parameters are shown in Table 4.

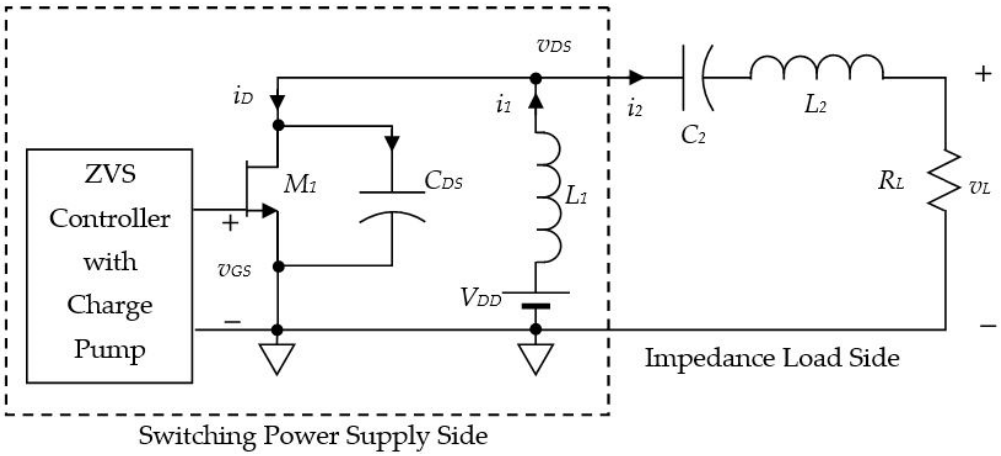

Figure 6. Class-E amplifier.

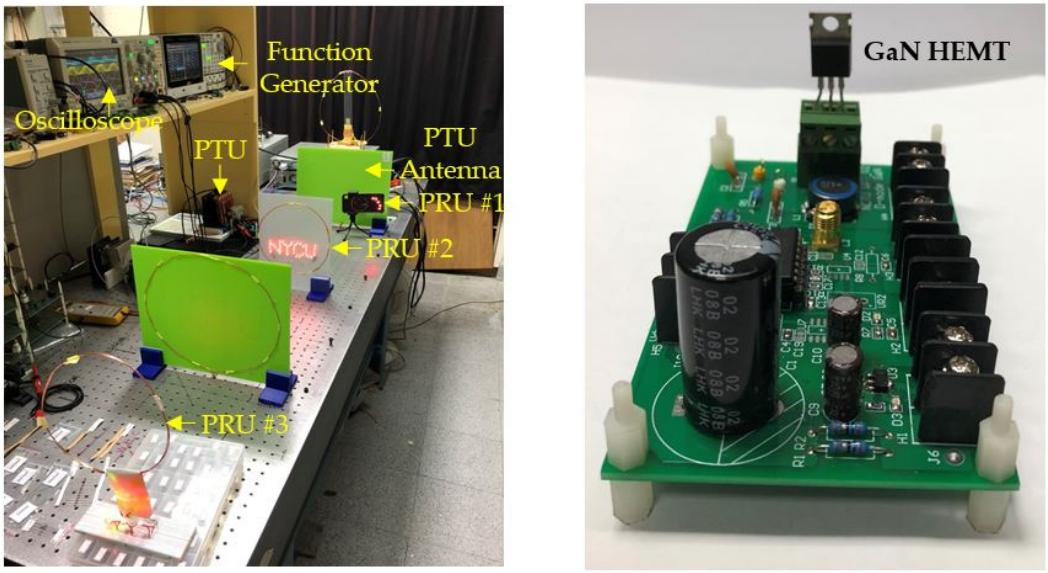

(**a**) (**b**)

Figure 7. (**a**) WPT experimental layout; (**b**) charge pump gate driver for D-mode GaN HEMT.

Table 4. Class-E amplifier equivalent parameters.

Symbol	Unit	Value
R_L	kΩ	5 [1]
C_{DS}	pF	100
C_2	pF	75
L_1	μH	47
L_2	μH	8

[1] Equivalent.

PWM Control and Circuit Response

In this study, the class-E amplifier circuit was considered in terms of two aspects: the switching power supply and impedance loading. The duty cycle of switching is denoted δ (i.e., the pulse width is δT (Figure 8a)). The SPICE analysis is shown in Figure 8b.

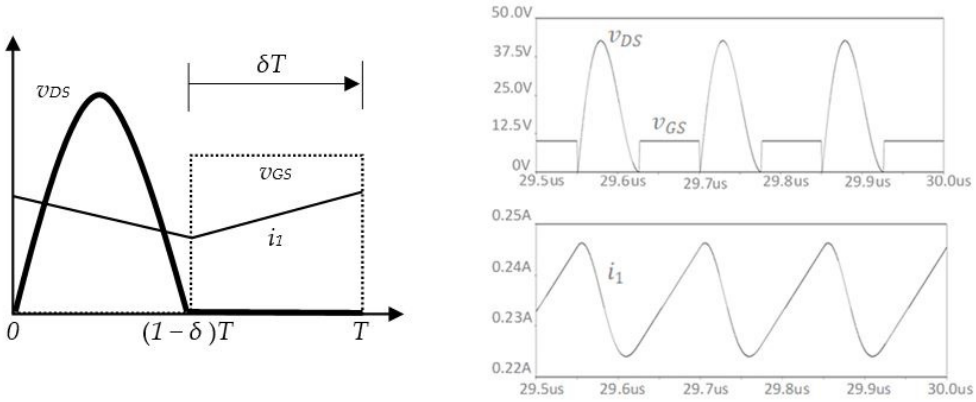

(a) **(b)**

Figure 8. (**a**) PWM control of D-mode GaN HEMT; (**b**) SPICE analysis.

The switch was operated at a frequency of $\omega_o = 2\pi/T$. In the steady state, the output current is $i_2 = I_2 \sin(\omega_o t + \beta) + I_{2,a} \cos(2\omega_o t + \beta)$. The higher order terms $I_{2,a} << I_2$ cause the sinusoidal output to be asymmetric on its upswing and downswing wave forms. An example in which $\beta = -180^\circ$, $I_2 = 1$, and $I_{2,a} = 0.15$, which are often seen in experiments, is shown in Figure 9a. The SPICE analysis is shown in Figure 9b.

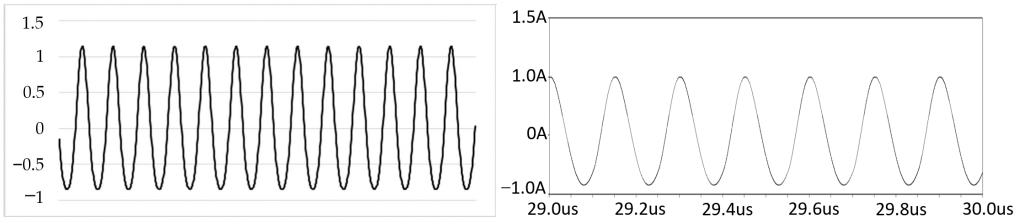

(**a**) (**b**)

Figure 9. Example of (**a**) i_2 current form. (**b**) SPICE analysis.

In practice, the v_{GS} signal of the class-E amplifier, as shown in Figure 10, is different from that of the SPICE analysis simulation. The output signal from the gate drive was no longer a square wave when the gate driver input signal from the PWM was a square wave between 0 and 5 V. The distortion of the gate drive output v_{GS} is due to the input parasitic capacitance Ciss. Since the Ciss is relatively small at the high drain-source voltage v_{DS}, as shown in Figure 3, compared to the Ciss at the low drain-source voltage, the turn-off delay time $t_{d,off}$ is therefore larger than the turn-on delay time $t_{d,on}$. The actual duty ratio is larger than the designed duty ratio. Thus an emperical result, and not just the SPICE model simulation result alone, was required to compensate in the design. Knowledge about the device characteristics, especially the parasitic capacitance variation resulting from different packaging and different switching frequencies, is essential to control resonant WPT via a class-E amplifier.

2.4. Maximum Power Transfer

The equivalent circuit of the wireless power transfer for a single PTU transferring power to a single PRU is shown in Figure 11. The resonant frequency ω_o was selected to yield the best impedance matching between $Z_{PTU}(j\omega_o)$ and $Z_{PRU}(j\omega_o)$ in order to obtain the maximum power transfer, which is also referred to as the maximum amount of power delivered to the load (PDL). The equivalent turn ratio a within the equivalent circuit for the wireless power transfer is a function of the distance between PTU and PRU. Hence, ω_o must be controlled from time to time to achieve the impedance matching condition when the PRU is moving. In a closed loop control, to tune the resonant frequency ω_o, the Airfuel

Alliance recommends obtaining the required feedback of the actual power reading of the PRU via a 2.4 GHz communication network.

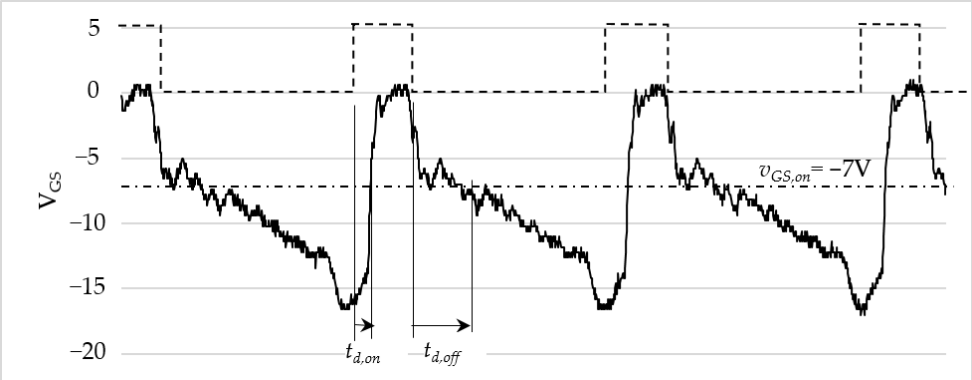

Figure 10. The comparison of the gate driver input (dotted line) and actual gate-source voltage output (solid line).

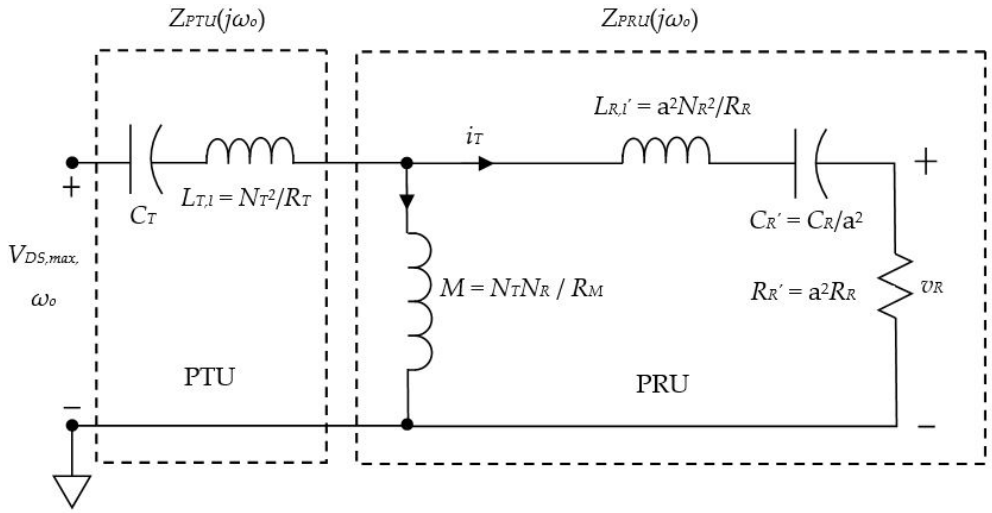

Figure 11. Wireless power transfer equivalent circuit.

The PDL is also a function of $V_{DS,max}$ of the switching power supply circuit shown in Figure 6. We need a high $V_{DS,max}$ to enable linkage travel for the magnetic flux in the air, linking it to the PRU antenna coil. From [23], the $V_{DS,max}$ is derived into a function of the duty ratio δ, as shown in Figure 12. Theoretically, the $V_{DS,max}$ is a monotonically increasing function in terms of the duty ratio δ. On the other hand, while the switching loss of the D-mode GaN HEMT also increases with the $V_{DS,max}$, the power transfer efficiency degrades due to the high $V_{DS,max}$. The reason that the switching loss of the D-mode GaN HEMT increases is that the GaN HEMT has no body diode. There is really only one disadvantage of the GaN HEMT having no body diode: a higher reverse voltage drop. The reverse voltage drop of a GaN HEMT includes a resistive element arising from the channel resistance and threshold voltage. The voltage drop in a high voltage GaN HEMT can be as much as several volts when conducting large currents, which is larger than the equivalent drop in a MOSFET. Thus, we have a situation in which there is a trade-off between a high PDL and a high switching loss in terms of the duty ratio δ.

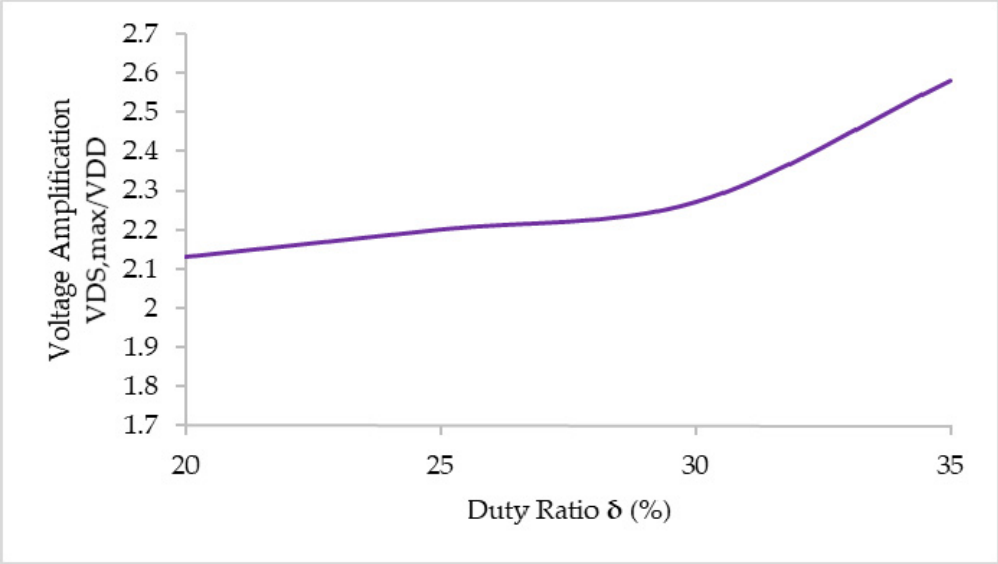

Figure 12. $V_{DS,max}$ vs. duty ratio.

In practice, when we monitor the power input of the PTU, we see the power input increase due to either the mismatching of the impedances, resulting in low PDL in the low duty ratio δ region, or the high switching loss from the high $V_{DS,max}$ in the high duty ratio δ region. The minimum power input, which trades off both deficiencies, is the optimal solution. In the following section, we introduce an empirical technique to locate the optimal duty ratio δ and achieve the best power transfer efficiency, which implies the high PDL associated with a low switching loss.

2.5. Minimum Power Input Control

The minimum power input control of a class-E amplifier can be obtained experimentally. A specific power transmitter unit, with its equivalent parameters, is detailed in Table 4. We completed a set of 70 experiments and interpolated the results (Figure 13). In the experiments, V_{DD} = 108 V, nominal resonant frequency = 4.12 MHz, and $\delta_{\%}$ (nominal duty ratio) = 30%. We calculated the minimum power points, which are indicated by red dots in Figure 13 and corresponded to the lowest power loss from C_{oss} to the ground in the switching. The experiment was extended to different input voltages V_{DD}. The results are shown in Figure 14. In WPT applications, higher input voltages V_{DD} are required for greater power transfer distances. Conversely, power input P_{in} increases with the distance between the PTU and power receiver unit (PRU). Furthermore, in cases of multiple PRUs, the power input P_{in} must be increased accordingly to supply sufficient power to the PRUs. We thus formulated our minimum control strategy according to the following steps:

(1) Due to the power transfer query issued by the PRU, we determined the input voltage V_{DD} according to the measured distance between the PTU and PRU.

(2) Due to the immediate power input P_{in} required for all PRUs, we determined the duty cycle δ (or duty ratio) according to the empirical data in Figure 14.

(3) From the duty ratio $\delta_{\%}$ calculated in step 2, we determined the resonant frequency f_0 according to the empirical data in Figure 15.

The minimum power input P_{in} is supplied to the WPT based on the empirical data or equations in Figures 14 and 15, which guarantees optimal power transfer efficiency. The minimum power input control is equivalent neither to conventional ZVS nor to zero current switching because of the absence of a body diode in the D-mode GaN HEMT. The energy stored in the C_{DS} is not released to ground when v_{DS} is negative. However, the minimum power input control minimizes the energy stored in the C_{DS} when the gate is turned on, which is like the ZVS control. A more important feature of our design is that almost all energy loss in the class-E amplifier is due to switching loss. Thus, the power loss

on the transistor switched-off time, which is the product of the drain current with the v_{DS}, is the key factor affecting the minimum power input control. The power loss is related to the gate drive design and the parasitic capacitance of the D-mode GaN HEMT; it is also absent in conventional ZVS control derivations.

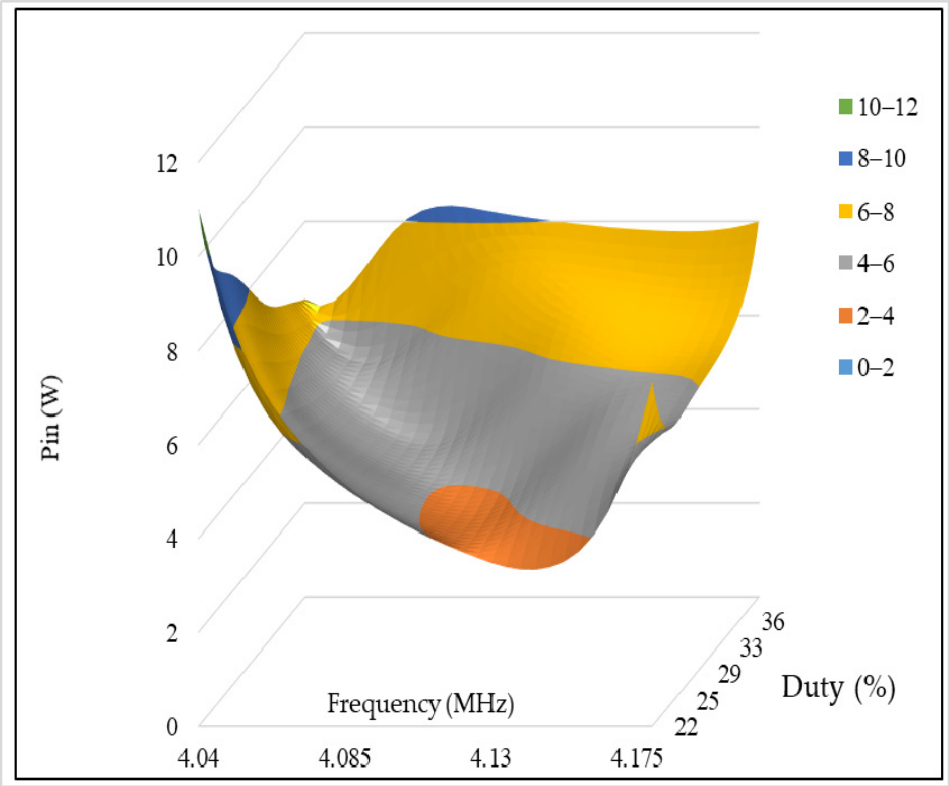

Figure 13. Input power due to different resonant frequencies f_0 and duty ratios $\delta_{\%}$ for V_{DD} = 108 V.

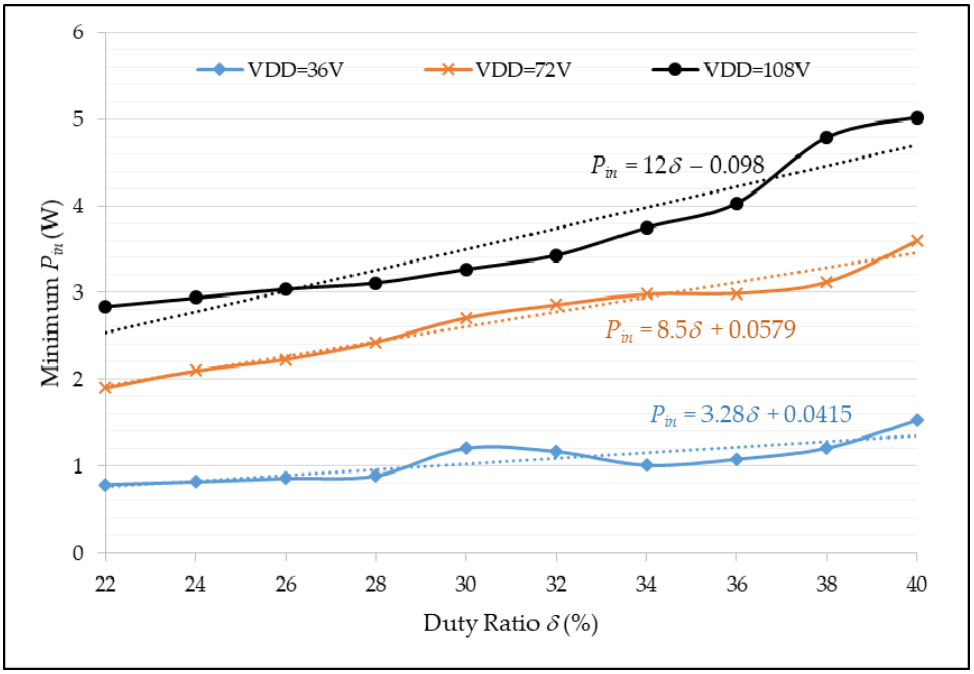

Figure 14. Minimum power input vs. the duty ratio $\delta_{\%}$.

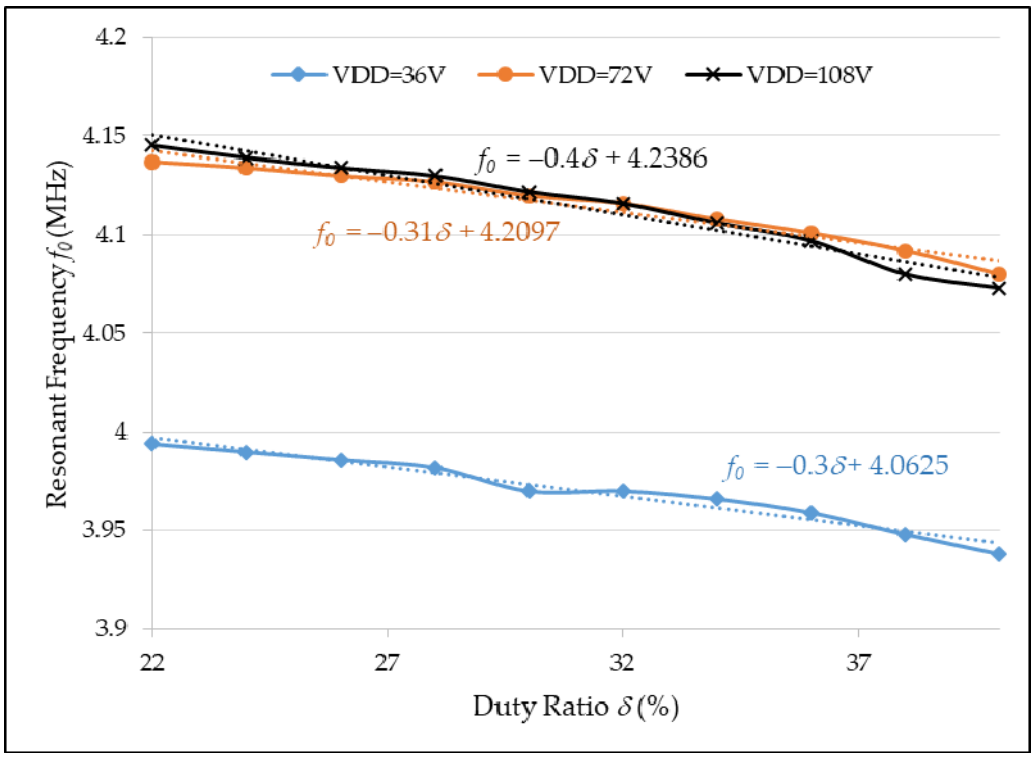

Figure 15. Resonant frequency f_0 vs. the duty ratio $\delta_{\%}$ under the minimum power input control.

3. Resonant WPT Results

As shown in Figure 16, a single PTU for the resonant WPT based on the D-mode GaN HEMT class-E amplifier was capable of transferring 1 W of power to a PRU 140 cm away. In the experiment, the load comprised 44 LEDs in series, each of which had a nominal power of 0.06 W. The maximum voltage $V_{DS,max}$ was 700 V, and the maximum current i_D was 2.5 A. The radii of the coils for both PTU and PRU were approximately 25 cm. When the PRU was 50 cm from the PTU, the PRU received 5 W power from the PTU (Figure 17). Due to the different distances between the PTU and PRUs in the WPT application, the maximum voltage $V_{DS,max}$, which is proportional to the duty cycle δ, must be adjusted to send power at an optimal efficiency. The minimum power input control was applied for this purpose according to the look-up table. The maximum voltage $V_{DS,max}$ is typically triple the input voltage V_{DD} in practice. Hence, the breakdown voltage of the D-mode GaN HEMT had to be higher than 1000 V for the application of 220 V_{AC}, which was rectified to 310 V_{DC}. Figure 18 shows the performance comparison of the PTE (%) in terms of transmission distance (cm). The method proposed in this paper yields performance comparable to the WPT with NIC method [24] with, however, no additional impedance transformation network circuit.

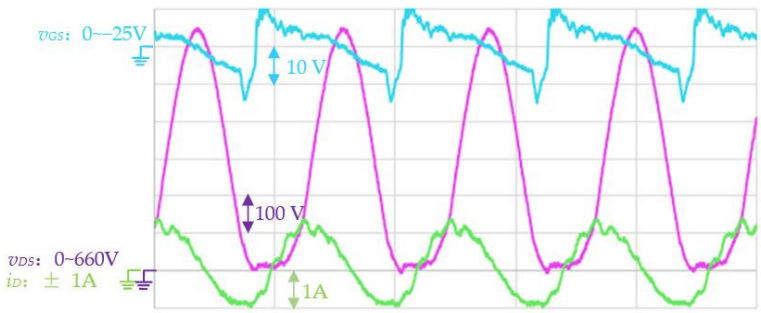

Figure 16. Data log of the class-E amplifier at 40 W at V_{DD} = 262 V.

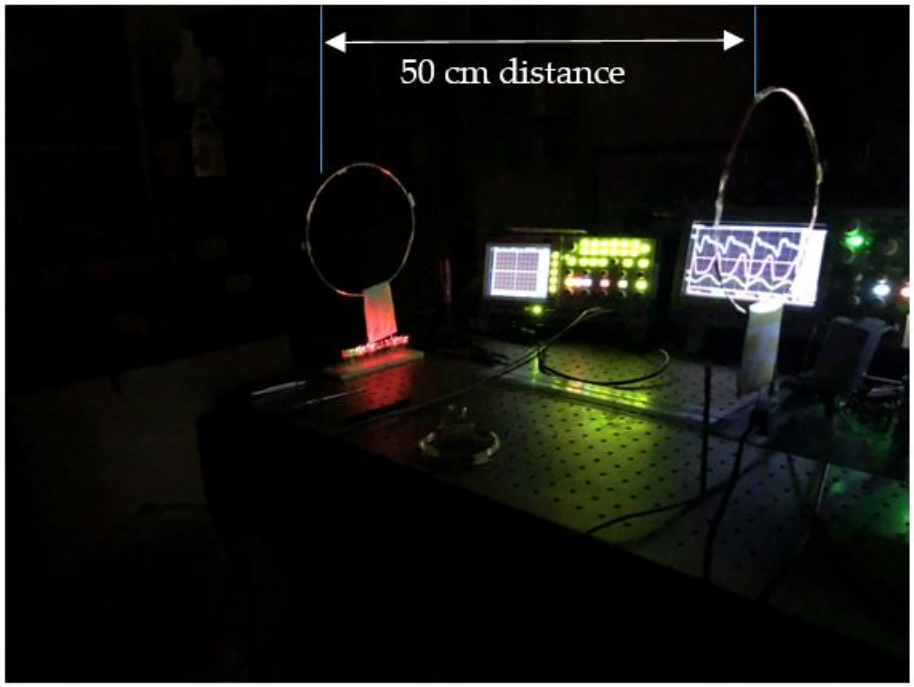

Figure 17. Example of 5 W at a 50 cm distance between the PTU and PRU.

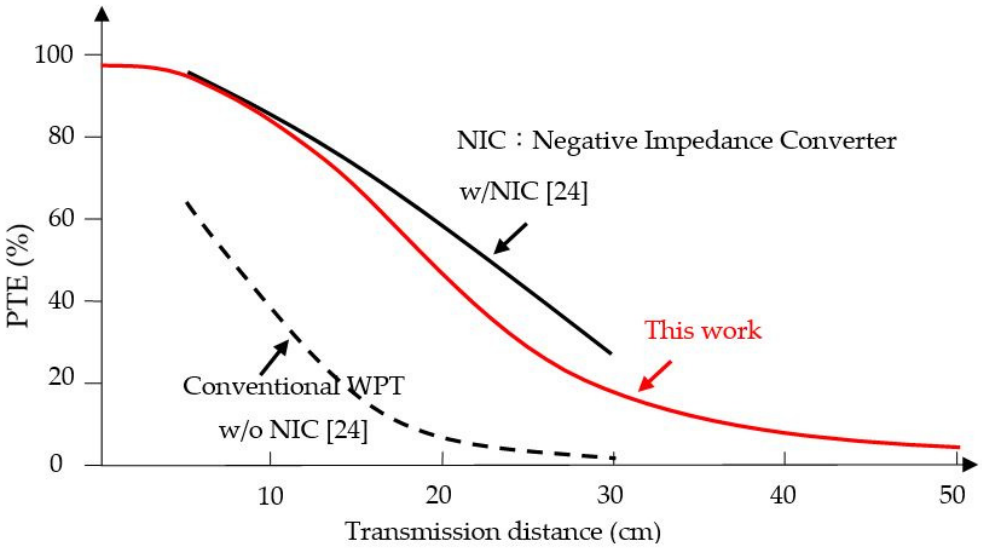

Figure 18. The performance comparison of the PTE (%) vs. transmission distance (cm).

4. Conclusions

The D-mode GaN HEMT fabricated at the authors' university, the National Chiao Tung University, was successfully implemented into the class-E amplifier circuit. The design of the D-mode GaN HEMT gate drive for the wireless power transfer is sensitive to parameters including the gate-drain parasitic capacitance *Crss* (=C_{GD}) and the gate input parasitic capacitance *Ciss* (=C_{GD} + C_{GS}). These parasitic capacitances of the GaN HEMT are essential for higher frequency switching with low switching loss. In the circuit design aimed at achieving the maximum power transfer, the corresponding impedance matching control was obtained in this research via adjustment of the resonant frequency ω_o,. Nevertheless, by controlling the duty ratio δ, a minimum power input control that trades off the power delivered to load for the switching loss of the GaN HEMT was obtained and found to yield good power transfer efficiency. The resulting resonant WPT was capable of transferring 1 W over the 140 cm distance between the PTU and PRU. Our minimum

power input control is an empirical method that generates a look-up table to optimize efficiency in WPT applications. In the future, the proposed design will be implemented for multiple-input and multiple-output (MIMO) applications—i.e., multiple PTUs serving multiple PRUs, which need to obtain the proper optimization method from among their individual look-up tables—via a 2.4 GHz communication network (recommended by the Airfuel Alliance) in order to improve the efficiency of power transfer.

Author Contributions: Conceptualization, E.L.C. and W.-H.C.; methodology, Y.-C.W.; software, C.-C.W.; validation, Y.-C.W., C.-C.W.; formal analysis, Y.-C.W.; resources, Y.-C.W.; writing—original draft preparation, W.-H.C.; writing—review and editing, C.-C.W.; visualization, E.L.C.; supervision, E.L.C.; project administration, E.L.C.; funding acquisition, W.-H.C. All authors have read and agreed to the published version of the manuscript.

Funding: This research was funded by the Ministry of Science and Technology, R.O.C, grant number MOST(NSC)109-3116-F009-001-CC1.

Institutional Review Board Statement: Not applicable.

Informed Consent Statement: Not applicable.

Data Availability Statement: Data sharing is not applicable.

Acknowledgments: This work was supported by the Ministry of Science and Technology, R.O.C. The authors would also like to thank CSD Lab for the fabrication of D-Mode MIS-HEMT chips, and IM Lab graduate students Ching-Yao Liu, Guo-Bin Wang, and Yue-Cong Sie for their help in the experiment setup.

Conflicts of Interest: The authors declare no conflict of interest.

References

1. Sokal, N.O.; Sokal, A.D. Class E—A new class of high-efficiency tuned single-ended switching power amplifiers. *IEEE J. Solid State Circuits* **1975**, *SSC-10*, 168–176. [CrossRef]
2. Liu, M.; Zhao, C.; Song, J.; Ma, C. Battery Charging Profile-Based Parameter Design of a 6.78-MHz Class E^2 Wireless Charging System. *IEEE Trans. Ind. Electron.* **2017**, *64*, 6169–6178. [CrossRef]
3. Aldhaher, S.; Mitcheson, P.D.; Arteaga, J.M.; Kkelis, G.; Yates, D.C. Light-weight wireless power transfer for mid-air charging of drones. In Proceedings of the 2017 11th European Conference on Antennas and Propagation (EUCAP), Paris, France, 19–24 March; pp. 336–340.
4. Chen, W.T.; Chinga, R.A.; Yoshida, S.; Lin, J.; Hsu, C.K. A 36 W wireless power transfer system with 82% efficiency for LED lighting applications. *Trans. Jpn. Inst. Electron. Packag.* **2013**, *6*, 32–37. [CrossRef]
5. Chokkalingam, B.; Padmanaban, S.; Leonowicz, Z.M. Class E power amplifier design and optimization for the capacitive coupled wireless power transfer system in biomedical implants. *Energies* **2017**, *10*, 1409.
6. Paolucci, M.; Green, P.B. Benefits of GaN e-Mode HEMTs in Wireless Power Transfer—GaN Power Devices in Resonant Class D and Class E Radio Frequency Power Amplifiers. October 2018. Rev 1.0. Infineon, White Paper. Available online: https://www.infineon.com/wirelesscharging (accessed on 17 October 2018).
7. Green, P.B. Class-E Power Amplifier Design for Wireless Power Transfer. August 2018. Rev 1.2. Infineon, Appl. Note 1803. pp. 1–51. Available online: https://www.infineon.com/wirelesscharging (accessed on 10 August 2018).
8. Akuzawa, Y.; Ito, Y.; Ezoe, T.; Sakai, K. A 99%-efficiency GaN converter for 6.78 MHz magnetic resonant wireless power transfer system. *J. Eng.* **2014**, *10*, 598–600. [CrossRef]
9. Lee, S.H.; Yi, K.P.; Kim, M.Y. 6.78-MHz, 50-W wireless power supply over a 60-cm distance using a GaN-based full-bridge inverter. *Energies* **2019**, *12*, 371. [CrossRef]
10. Yeh, C.H.; Lin, Y.T.; Kuo, C.C.; Huang, C.J.; Xie, C.Y.; Lu, S.F.; Yang, W.H.; Chen, K.H.; Lin, Y.H. A 70W and 90% GaN-based class-E wireless-power-transfer system with automatic-matching-point-search control for zero-voltage switching and zero-voltage-derivative switching. In Proceedings of the 2018 IEEE International Solid-State Circuits Conference-(ISSCC), San Francisco, CA, USA, 11–15 February 2018; pp. 138–140.
11. Xie, C.Y.; Yang, S.H.; Lu, S.F.; Lin, F.Y.; Lin, Y.A.; Ou-Yang, Y.Z.; Chen, K.H.; Liu, K.C.; Lin, Y.H. 15.3 A 100W and 91% GaN-Based Class-E Wireless-Power-Transfer Transmitter with Differential-Impedance-Matching Control for Charging Multiple Devices. In Proceedings of the 2019 IEEE International Solid-State Circuits Conference-(ISSCC), San Francisco, CA, USA, 17–21 February 2019; pp. 242–244.
12. Grebennikov, A. Load Network Design Techniques for Class E RF and Microwave Amplifier. *High Freq. Electron.* **2004**, *3*, 18–32.
13. Barman, S.D.; Reza, A.W.; Kumar, N. Coupling Tuning Based Impedance Matching for Maximum Wireless Power Transfer Efficiency. *J. Comput. Sci. Comput. Math.* **2016**, *6*. [CrossRef]

14. Jiang, C.; Chau, K.T.; Liu, C.; Lee, C.H. An overview of resonant circuits for wireless power transfer. *Energies* **2017**, *10*, 894. [CrossRef]
15. Muharam, A.; Ahmad, S.; Hattori, R. Scaling-Factor and Design Guidelines for Shielded-Capacitive Power Transfer. *Energies* **2020**, *13*, 4240. [CrossRef]
16. Minnaert, B.; Costanzo, A.; Monti, G.; Mongiardo, M. Capacitive Wireless Power Transfer with Multiple Transmitters: Efficiency Optimization. *Energies* **2020**, *13*, 3482. [CrossRef]
17. Li, C.; Wang, B.; Huang, R.; Yi, Y. A Resonant Coupling Power Transfer System Using Two Driving Coils. *Energies* **2019**, *12*, 2914. [CrossRef]
18. Wen, F.; Li, R. Parameter Analysis and Optimization of Class-E Power Amplifier Used in Wireless Power Transfer System. *Energies* **2019**, *12*, 3240. [CrossRef]
19. Ng, W.T.; Yu, J.; Wang, M.; Li, R.; Zhang, W. Design Trends in Smart Gate Driver ICs for Power GaN HEMTs. In Proceedings of the 2018 14th IEEE International Conference on Solid-State and Integrated Circuit Technology (ICSICT), Qingdao, China, 31 October–3 November 2018; pp. 1–4.
20. Ishibashi, T.; Okamoto, M.; Hiraki, E.; Tanaka, T.; Hashizume, T.; Kikuta, D.; Kachi, T. Experimental validation of normally-on GaN HEMT and its gate drive circuit. *IEEE Trans. Ind. Appl.* **2014**, *51*, 2415–2422. [CrossRef]
21. Chou, P.C.; Cheng, S. Performance characterization of gallium nitride HEMT cascode switch for power conditioning applications. *Mater. Sci. Eng. B Adv.* **2015**, *198*, 43–50. [CrossRef]
22. Wu, C.C.; Jeng, S.L. Simulation Model Development for Packaged Cascode Gallium Nitride Field-Effect Transistors. *Crystals* **2017**, *7*, 250. [CrossRef]
23. Liu, C.Y.; Wang, G.B.; Wu, C.C.; Chang, E.Y.; Cheng, S.; Chieng, W.-H. Derivation of the Resonance Mechanism for Wireless Power Transfer Using Class-E Amplifier. *Energies* **2021**, *14*, 632. [CrossRef]
24. Kim, T.-H.; Yun, G.-H.; Lee, W.; Yook, J.-G. Highly efficient WPT system with negative impedance converter for Q-factor improvement. *IEEE Access* **2019**, *7*, 108750–108760.
25. Liu, S.; Liu, M.; Fu, M.; Ma, C.; Zhu, X. A high-efficiency Class-E power amplifier with wide-range load in WPT systems. In Proceedings of the 2015 IEEE Wireless Power Transfer Conference (WPTC), Boulder, CO, USA, 13–15 May 2015; pp. 1–3. [CrossRef]